MRI RECONSTRUCTION USING COMPRESSED SENSING WITH LOCAL BINARY PATTERN FOR MULTI-DOMAIN VIA CONVOLUTION NEURAL NETWORK

D. M. Annie Brighty Christilin[1] and **Dr. M. Safish Mary[2]**

1.Research Scholar, Reg No: 17221282162004, Department of Computer Science, St. Xaviers College, Affiliated to Manonmaniam Sundaranar University, Abishekapatti, Tirunelveli, Tamil Nadu, India,
2. Assistant Professor, Department of Computer Science, St Xaviers College, Affiliated to Manonmaniam Sundaranar University, Abishekapatti, Tirunelveli, Tamilnadu, India

ABSTRACT:
Compressed Sensing method suppress the MRI acquisition time for considering the patient's health. So the sensing process is carried out by a way of projecting an under-sampled data from spatial and k-space domain simultaneously. In this paper, our proposed Multi-domain reconstruction net acquires the under-sampled data with local binary pattern at the different sampling rates and reconstructs the resultant under-sampled data through the MD-USLBPRNET. Our proposed MD-USLBPRNET consists of two parallel channel and act together sections and also execute on spatial and k-space domain data simultaneously. Experimentally, the proposed method shows the performance better than the existing Deep learning method with the qualitative metric such as Peek-Signal-to-Noise Ratio and Structural Similarity Index.

Keywords: Compressed Sensing, Local Binary Pattern, MRI Reconstruction, Multi-domain Reconstruction Net

1. Introduction

Magnetic resonance imaging technology is noninvasively for gathering the information about physiological functions of human body. MRI is excellent for other modalities like soft-tissue contrast and resolution. But in k-space, the sampling process of MRI suffers from the patient's health for long time acquisition due to physiological and hardware constraints. So this long time acquisition creates some artifacts for reducing the image quality. These problem make an unsuitable diagnosing a time-critical disease like stroke [1]. So MRI reconstruction method is implemented by Compressed Sensing.

CS joins compression and sensing or acquisition. Here the under-sampled data are collected at a few numbers of measurements [2]. The high dimensional data is analyzed in medical regions such as MRI and CT, audio or video or image [3]. So the CS mechanism is very important for this kind of analysis.

The compressed representation of the testing signal is held by CS sensing mechanism. It is examined by sensing or projection matrix. A well-known algorithm like Basis Pursuit [4] is a predictable CS method and provides the time complexity of the number of measurements $O(s \log (n/s))$ in the n-dimensional s-sparse signal based on Gaussian random matrices [5]. The significant problem of BP that random matrices are typically considered to build hardware is complicated. Also, arbitrary matrices multiply with signal vectors of high dimension. If there is no fast matrix multiplication algorithm, it evaluates the high computation cost. In this article, a new CNN method proposes reconstructing the image for the fusion of spatial and frequency under-sampled data.

Related review and the proposed network are described in Section 2 and 3. The experimental results are evaluated for the existing and proposed methods that are highlighted in Section 4. Finally the conclusion is represented in this paper.

2. Literature Review

Many developed CS algorithms reduce the acquisition time in MRI. Firstly, the hardware-based parallel MRI (pMRI) [6] algorithm, which may be measured raw data from an individual tissue type with the help of phased array coils, which contains multiple independent receiver channels [7]. The pMRI reconstruction methods are classified into three types such as image domain-based methods SENSE with its variants [8] [9], k-space based methods SMASH [10] and GRAPPA [11], and combinations of the previous two kinds of ways, such as SPACE-RIP [12] and SPIRiT [13]. In wide clinical application, the pMRI still has modest acceleration rates.

In compressed sensing magnetic resonance imaging (CS-MRI) [14,15] , the acceleration rate is proportional to the sampling ratio. CS-MRI attempts to get faster reconstruction with under-sampled k-space data at a lower rate than the one set by the classical Nyquist-Shannon sampling theorem. In CS-MRI, the image is sparsified by a certain sparsifying transform like Fourier transform (FT), wavelet, total variation (TV), and low-rank[16] before the image is reconstructed. Currently, the two data-driven CS methods have been improved the CS-MRI performance [17] such as dictionary learning and transform learning. Although these methods have achieved several critical drawbacks still slow down the clinical practice of CS-MRI. Because the major issues are time-consuming iteration and also high computation cost. The regular process cannot guarantee constantly advanced performance for all scanning protocols and patients because of the need of precise preceding information.

3. Existing Method:

According to data processing and specific pipeline, the fast MRI methods can be classified into five groups based on Deep Learning. The main gathering is post-preparing calculations that utilization the inverse Fourier Transform (IFT) to get an underlying picture as the previously contribution to the organization. In this gathering, the organization model demonstrates the job of a picture to-picture planning capacity. The soonest strategy [18] presents a generative ill-disposed organization (GAN) into post-handling based quick MRI reproduction. DAGAN [19] adds an information consistency layer to guarantee the focuses on the reasonable information complex. DAGAN-Cyclic misfortune [20] is utilized as a more profound generator and discriminator network with cyclic information consistency misfortune to additional improve imaging quality. This sort of technique is the standard of current DL-based models, as it is helpful to embed into the current work process of business scanners.

The second step denotes the below average straightforwardly manages the under-sampled k-space information utilizing a neural organization, and from that point onward, IFT is applied to get the eventual outcomes [21]. Since any relics presented by the organization may spread to the entire reproduced picture, this sort of technique has not yet been generally contemplated. The third Step such as the emphasis unrolling techniques [22]. In particular, in [23], the information consistency layer was inserted into the unrolling cycle organization, and a similar gathering improved the previous organization by presenting enlarged convolution and stochastic design [24].

Distinctive iterative mathematical solvers are treated as different intermittent organizations in these techniques, and the learned regularization terms compel the picture regarding each halfway remade result. The fourth step incorporates strategies that straightforwardly take in the picture from the under-sampled k-space information [25]. Completely associated layers are typically required for this sort of model, and the organization scale is by and large

gigantic. All the referenced techniques acted in a solitary area have not completely investigated the idle connection between k-space and the spatial area. The last step has acquired a lot of consideration as of late. This technique endeavors to investigate the data in both the k-space and the spatial area [26]. It as a rule receives two fell organizations performing on k-space and spatial-area information, with IFT utilized to fabricate the scaffold between the two organizations.

Different iterative numerical solvers are treated as various recurrent networks in these methods, and the learned regularization terms constrain the image in terms of each intermediate reconstructed result. Fig. 1(d) includes techniques that directly learn the image from the under-sampled k-space data. Fully connected layers are usually needed for this kind of model, and the network scale is generally massive. All the mentioned methods performed in a single domain have not fully explored the latent relationship between k-space and the spatial domain. The last step has gained much attention very recently. This method attempts to explore the information in both the k-space and the spatial domain. It usually adopts two cascaded networks performing on k-space and spatial-domain data, with IFT employed to build the bridge between the two networks.

Currently, state-of-the-art performance is achieved using such dual-domain based methods. However, existing dual-domain methods [27] executes the k-space and spatial-domain data sequentially, which implicitly adds a certain priority priori into the reconstruction and may ignore the internal interplay between both domains. In this paper, the intrinsic relation between the k-space and spatial domains be noticed, a novel MRI Dual-domain Reconstruction Network (MD-DLLBPRNet) is proposed to accelerate magnetic resonance imaging. Unlike current methods, the proposed MD-DLLBPRNet contains two parallel and interactive branches that simultaneously operate on k-space with Local Binary Pattern descriptor and spatial-domain data. Data consistency layers are included to improve performance further. In the end, dual-domain fusion layers combine the results from the two branches.

4. Proposed MD-DLLBPRNET Architecture

In this proposed architecture [Fig.1], let's take the input data from fully and under-sampled image. However, the fast Fourier transform apply on the fully image to get a fully k-space image. Next the mask of that image multiplies with a temporary image to get an under-sampled k-space image. Lets apply the inverse fast Fourier transform into the insensitive LBP image portion which has feature extractor parameter x (less than 128) for getting a normalized under-sampled image. And also the sensitive LBP image portion which has feature extractor parameter y (greater than 128) preserve the structure itself. Finally the under-sampled image obtain for spatial and frequency domain. Let's take these resultant under-sampled images as input data for the proposed MD-USLBPRNET architecture to enhance its image quality.

4.1 Formation of LBP Image

The traditional LBP operator [28] works on image patches of size 3 X 3, 5 X 5, etc. The neighboring pixel intensity is compared to that of the central pixel within the patch sequentially for forming the LBP descriptor. If the central pixel's higher intensity values are compared to the neighboring pixel, the value 1 is assigned or otherwise 0. Finally, these bit string is converted to a decimal number (using base 2) as the feature value assigned to the central pixel. These cumulative feature values characterize the local texture in the image. The LBP for the center pixel (x_c, y_c) within a patch can be represented as

$$LBP(x_c, y_c) = \sum_{n-0}^{L=1} s(i_n, i_c) \cdot 2^n \qquad (1)$$

Where i_n denotes the intensity of the nth neighboring pixel, i_c denotes the intensity of the central pixel, L is the length of the sequence, and $s(\cdot) = 1$ if i_n i_c and $s(\cdot) = 0$ otherwise. For example, a N x N neighborhood consists of $N^2 - 1$ neighboring pixels and therefore results in an $N^2 - 1$ long bit string. The different parameters and configurations of the LBP formulation can result in different feature descriptors. Thus, the texture image is found using the LBP descriptor adaptive parameter. Let us reformulate the LBP encoding more efficiently using filters. The traditional implementations of encoding LBP features use a 3 x 3 window to scan through the entire image in an overlapping fashion. At each 3 x 3 patch, the encoding involves (1) compute the difference between the pivot and the neighboring pixels (or pairs of pixels more generally), (2) a non-linear thresholding operation mapping the pixel differences to binary values, and (3) pooling the binary values through a weighted sum. Each filter is a 2-sparse difference filter. The 8 resulting bit maps after binarization are also found. Standard formulations of LBP are simply a weighted sum of all the bit maps using a predefined weight vector $v = [2^7, 2^6, 2^5, 2^4, 2^3, 2^2, 2^1, 2^0]$.

Therefore, standard LBP feature extraction can be reformulated as $y = \sum_{i=1}^{8} (b_i * x) \cdot v_i$.

Where, $x \in R^d$ is the original image's vectorized version.

b_i's are the sparse filters.

be the non-linear binarization operator.

$y \in R^d$ be the resulting LBP image.

By appropriately changing the linear weights v, that can vary the base and the encoding ordering. Similarly, changing the non-zero {+1 and -1} support in the filters allows us to change the pivot. So the obtained scaling parameter x or y represents as based on texture image value either greater or less than a predefined threshold.
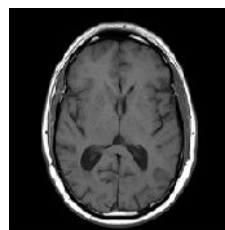
Gray Image   Texture Image

Let $y_f \in C^{mxn}$ be the fully sampled k-space data, and $y \in C^{mxn}$ be the corresponding under-sampled data.

Where, m and n are the image size. The under-sampled data and fully sampled data are reconstructed from zero-filling solution. The under-sampled data are represented as x_u x, x_f $y \in C^{mxn}$. The solution of image reconstruction can be formulated as:

$$y = U_{lbp} \odot y_f + \in \quad U_{lbp} \odot T(x_u \cdot x + x_f \cdot y) + \in = f_u(x_u \cdot x + x_f \cdot y) + \in \quad (2)$$

Where, T signifies the 2D FT operator. $U_{lbp} \in R^{mxn}$ represents the binary under-sampling mask with LBP. $f_u = U_{lbp} \odot T$ denotes the under-sampling Fourier encoding operator. $\odot$ is

element-wise multiplication. $\in$ is acquisition noise. The first relationship between spatial and frequency domain data indicates the accelerated MRI algorithm that focuses on this article. The ill-posed problem of Eqn.2 is solved by the classic basic model CS-MRI. The associated optimization problem can be expressed as the following variational minimization:

$$\min_{x} \; 1/2 \; f_u \left(x_{u\;x} + x_{f\;y}\right) - \text{as th follcwing} + (\; y_u\|_2^2 \quad \lambda R x) \tag{3}$$

Where $f_u\left(x_{u\;x} + x_{f\;y}\right) - y_u$ represents data fidelity. This solution signifies the data consistency between the reconstruction result and the proposed under-sampled k-space data. $R(x)$ denotes the regularization term that constrains the least-squares data fidelity term, and $\lambda >= 0$ is a balancing parameter that controls the tradeoff between that. Particularly, $R(x)$ is usually an l_0 norm or l_1 norm in a certain sparsifying transform field such as FT, wavelet, total variation (TV), and lowrank.

DL-based CS-MRI [29] makes the reconstructed image and the corresponding fully sampled image by optimizing the parameter set θ of the neural network. This method can be represented as:

$$\min_{x} \; 1/2 \; \|f_{nn}(z|\theta) - \left(x_{u\;x} + x_{f\;y}\right)\|^2 + \lambda \|f_u\left(x_{u\;x} + x_{f\;y}\right) - y_u\|_2^2 \tag{4}$$

Where f_{nn} is the network model with parameter set θ, z is the input of the model, either y_u or x_u, and $f_{nn}(z|\theta)$ is the output. Hence the resultant lbpunder-sampled image is forwarded to the extension of network architecture namely as Multi-domain Under-sampled Local Binary Pattern Reconstruction network for reconstructing the image.

Fig1. Proposed MD-DLLBPRNET Method
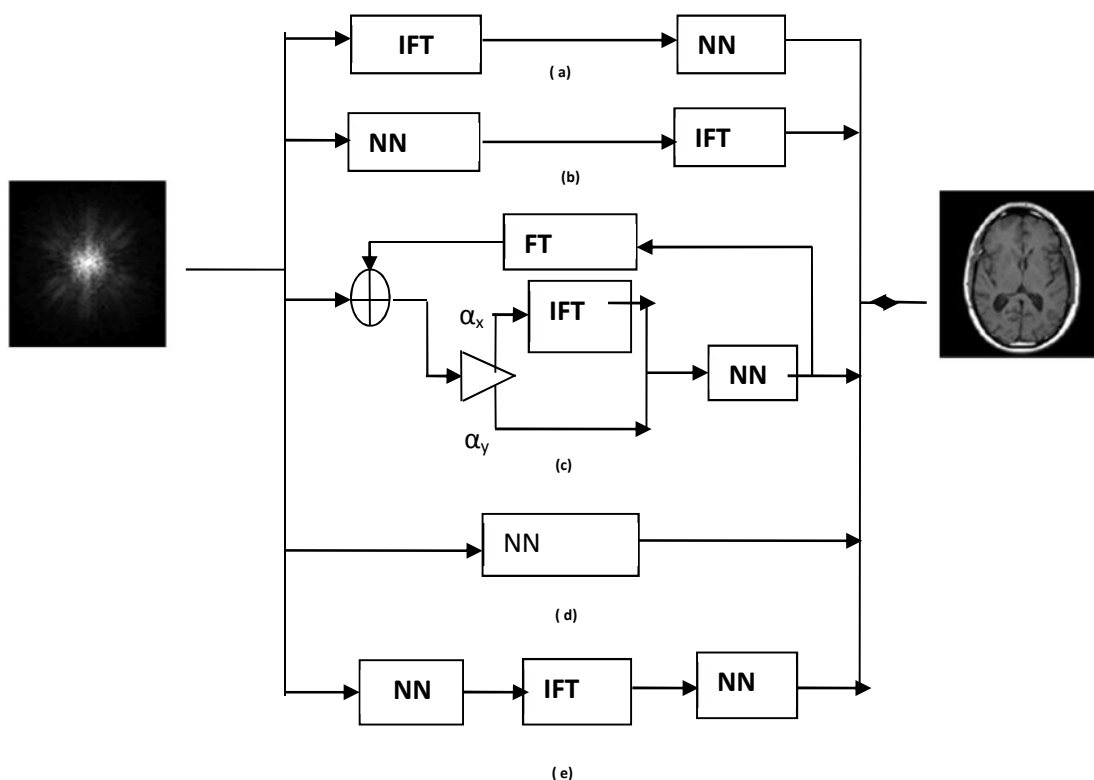
4.2.1 Extension MD-USLBPRNET Architecture

In this segment, the proposed MD-USLBPRNET Network Architecture shows in Fig. 2(a). It comprises of five essential squares, and all squares share a similar design with the exception of the last square. The organization takes both under-sampled k-space information y and zero-filling LBP reconstruction x_u as input and calculates the full-sampling reconstruction x. The proposed network contains two branches to deal with the k-space and spatial information independently. The essential handling block's overall structure delineate in Fig. 2(b) and 2(c). The block structure of the proposed technique is the principle commitment of this paper. The initial four block share a similar construction, which shows in Fig. 2(b). This block contains the accompanying segments: CNN, FT, IFT, k-space information consistency (KDC), spatial information consistency (SDC), k-space combination (KF), and spatial combination (SF) layers. Each block acknowledges two sources of info, k-space, and spatial information, and contains two CNN modules which are utilized to separate and recuperate the two domain's feature.

The subtleties of the CNN show in Fig. 2.(d). It comprises of 5 convolutional layers with 32, 32, 32, 32, and 2 channels, individually. Leftover association [30] quickens the preparation system and save more detail. Since MR information are mind boggling esteemed, two channels address the genuine and fanciful parts, separately. The first convolutional layer input contains two channels. The last convolutional layer just contains two filters. All kernels are set to 3 × 3 and follow by a LeakyReLU unit with a negative incline $1e-2$. The step sets to 1, and we keep the components of the information and yield steady by setting the estimation of padding=1. The two CNN modules' yields are taken care of into two diverse information consistency modules, for example, KDC and SDC. These CNN module force information imperatives on the two spaces' middle of the road results. From that point forward, FT and IFT are applied to the spatial and k-space information individually to get the outcomes from various areas. At that point, KDC and FT's yields are taken care of into the KF module, and the yields of SDC and IFT are taken care of into the SF module. At last, the KF and SF modules yield gives the middle of the road remade results. The last block, appeared in Fig. 2.(c), is like the past ones in Fig. 2.(b), with the lone contrast happening after the information consistency layers. Since this block fares the last recreated pictures rather than the double area results, the FT and KF modules are taken out, and the end-product is acquired after spatial combination. For effortlessness, mean square error (MSE) is embraced as the proposed organization's misfortune capacity, and it is characterized as:

$$L = 1/N \sum_{i=1} \|x_i - x'_i\|_2^2 \tag{5}$$

Where x' is the evaluated MR image of the network, and N denotes the total number of samples.

4.2.1.1 Data Consistency Module

A data consistency layer imposes the An information consistency layer force the limitations from the first estimations. The possibility of consistency consolidates the data fidelity into the neural network. Consequently the recipe for KDC as indicated by the shut structure arrangement of (3), as follows:

$S_{rec} (j) = y'(j) \; if \; j \notin \Omega$
$(y' + \; y(j))/(1+ v) \; if \; j \in \tag{6}$

Where, j represents the index of the vectorized representation of k-space data. y' denotes the evaluated k-space data from the previous CNN module. y signifies the under-sampled k-space data,   is the sampling index set, and   is a hyperparameter. In (6) if the k-space coefficients are not sampled ($j \notin \Omega$) the value predicted by the CNN module is used for the sampled entries, this is a linear weighted summation between the evaluated and original sampled data by CNN. SDC plays a similar role to KDC but performs in spatial domain. It can be implemented easily by adding FT and IFT before and after SDC. The forward and backward passes of KDC and SDC can be easily captured.

Fig. 2 Proposed MD-USLBPRNET Architecture

(d)
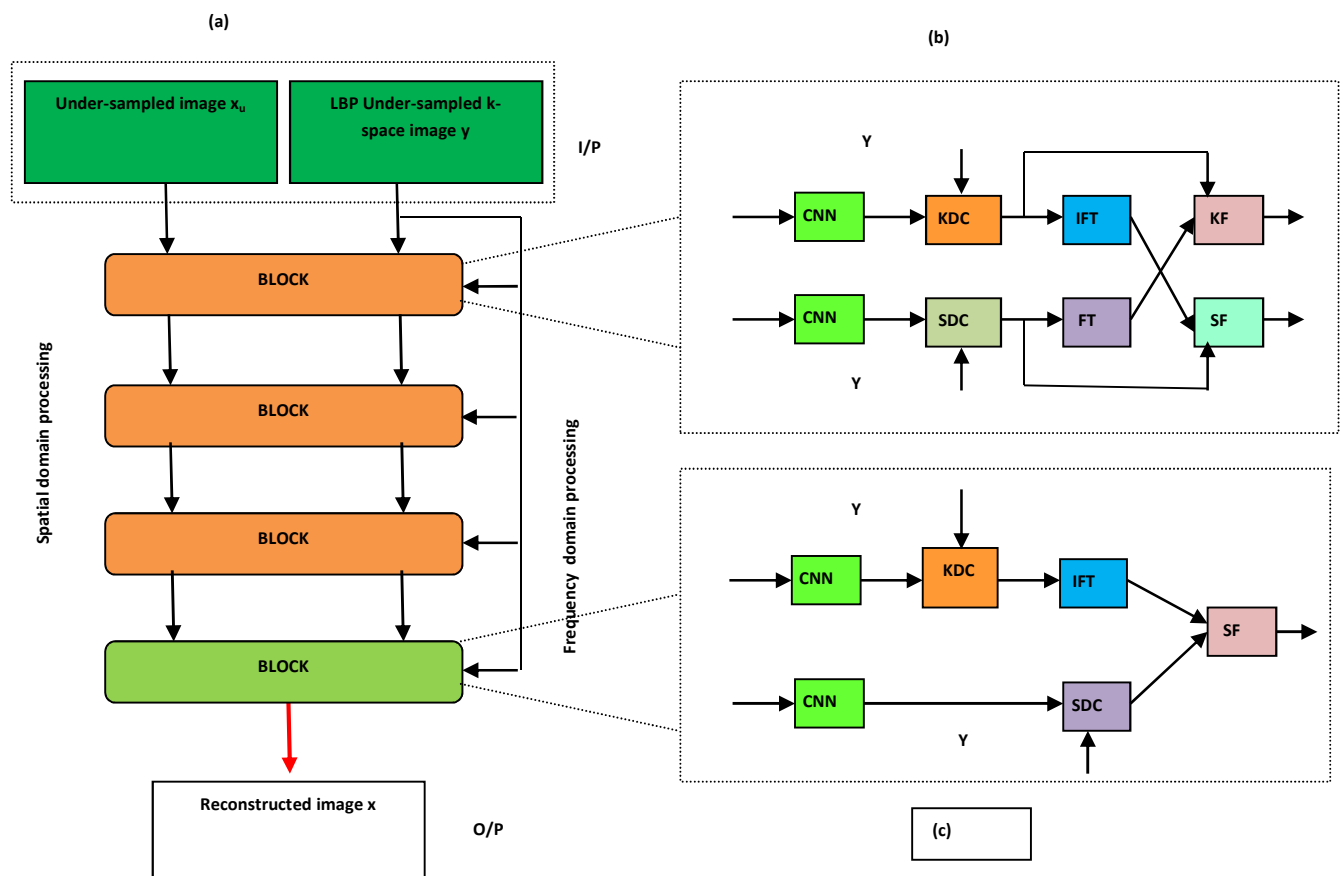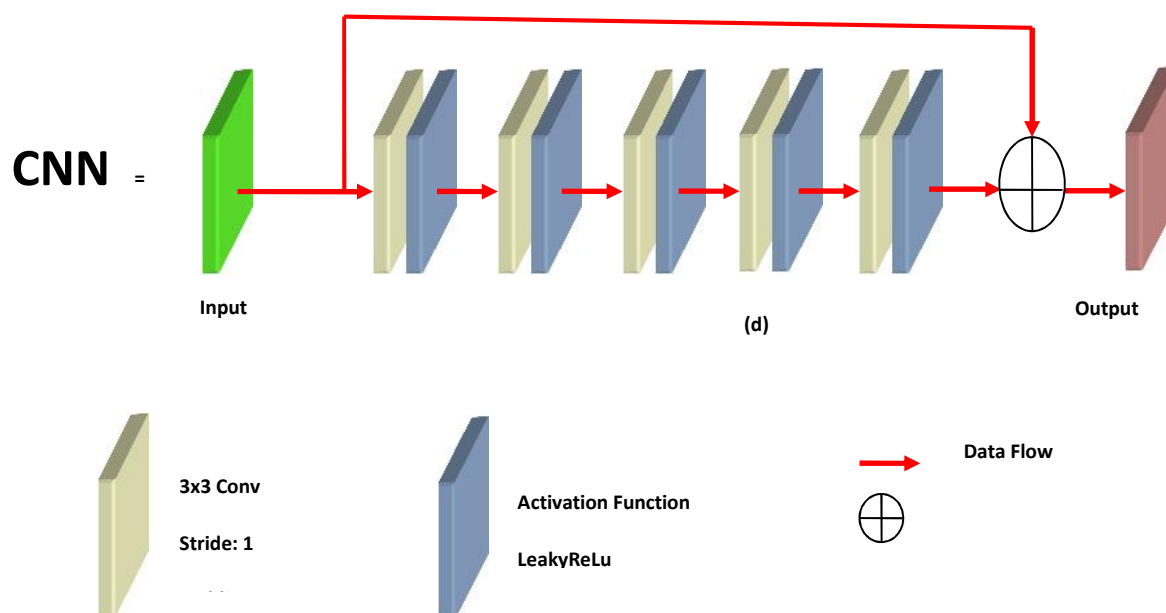
4.2.1.2 Data Fusion Module

As per the k-space method, the trial of this technique has preferred execution over k-space area organization; a few subtleties must be recuperated by k-space organization. In light of this perception, the proposed MD-USLBPRNet attempts to exploit the benefits in double areas and an equal intelligent design with two branches is utilized. One of the principle commitments in this paper is that the information from the two spaces are not independent, however intelligent by means of the combination modules. In Fig.2, two kinds of combination modules, KF and SF, are utilized. The formulae of two modules are same and the distinction lies in the pre-owned information structures. KF and SF modules separately manage the k-space and spatial information. KF module takes the yields of past KDC and FT as data sources and SF module takes the yields of past SDC and IFT as information sources. The calculations of KF and SF are gotten together with a straight blend between two information sources and can be defined as:

$A = (1/(1 + \mu)) A_1 + (\mu/(1 + \mu)) A_2$ (7)

Where A is the output of the fusion module, A_1 and A_2 are the inputs, μ is the balancing factor.

5. Experimental Result:

The T1w MRI DICOM image www.cancerimagearchive.net utilizes for training and testing set of our proposed model as Numpy image. In total, 5000 slices from 25 images are randomly selected to form the training set, and the testing set consists of 2000 slices from 10 other images. The size of the acquisition matrix is 256 × 256. Raw MR data are complex valued, but CNNs can only handle real numbers. Let's take the real and imaginary data as network input. The Adam optimizer utilize for optimizing this network, and its parameters are set as   = 5e–5,   1 = 0.9,   2 = 0.999.

The initial learning rate be 5e–5. The parameters   in (8) and μ in (9) are trained as network parameters. Here, three types of mask are generated. For radial sampling mask, 10%, 20%,

30%, 40%, 50%, 60%, 70%, 80%, 90% sampling rates are tested for under-sampling strategies. And only 10%, 20%, 30% sampling rates are tested for the other two types.

(a) Gaussian random mask	(b) Cartesian sampling mask	(c) radial sampling mask
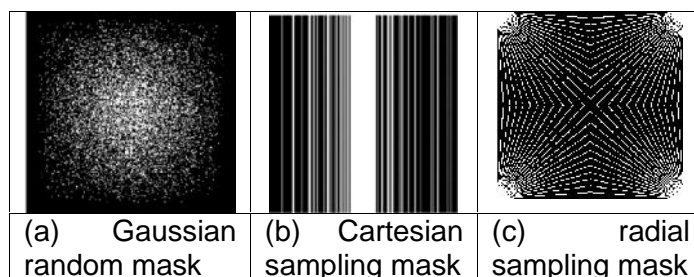
The performance of the existing and the proposed **MD- USLBPRNET method** evaluate by the qualitative metric such as SSIM and PSNR.

$$PSNR = 20 \log 10 \left(255 / \left(\left(1/mn\right) \sum_{i=0}^{m=1} \sum_{j=0}^{n=1} [I(i,j) - K(i,j)]^2 \right)^{1/2} \right) \quad (8)$$

$$SSIM = \frac{(2\mu_x \mu_{x'} + c_1)(2\sigma_{xx'} + c_2)}{(\mu_x^2 + \mu_{x'}^2 + c_1)(\sigma_x^2 + \sigma_{x'}^2 + c_2)} \quad (9)$$

Table1 shows that the performance of the existing and proposed method for 9 images with the PSNR and SSIM values for 20% radial sampling rates.				
Method	**Existing method**		**Proposed MD-USLBPRNET**	
Image id	**PSNR**	**SSIM**	**PSNR**	**SSIM**
1	31.40188	0.856319	32.92245	0.915825
2	35.73466	0.936572	30.93831	0.851122
3	30.48668	0.75989	36.07648	0.937305
4	34.56463	0.932973	30.5495	0.786049
5	31.75484	0.894262	34.16445	0.927882
6	28.95324	0.742213	30.86582	0.78054
7	29.8756	0.821782	34.13046	0.928236
8	31.8245	0.849145	32.80678	0.87528

Table2 shows that the performance of the existing and proposed method for 9 images with the PSNR and SSIM values for 20% Gaussian random sampling rates.				
Method	**Existing method**		**Proposed MD-USLBPRNET**	
Image id	**PSNR**	**SSIM**	**PSNR**	**SSIM**
1	29.57432	0.746466	27.47777	0.732222
2	30.78833	0.735555	28.32473	0.692377
3	28.57744	0.725525	25.47747	0.686665
4	32.45774	0.858588	30.59468	0.756667
5	28.57336	0.827477	23.58675	0.799836
6	27.66446	0.635456	25.47746	0.698387
7	24.84757	0.734666	21.47673	0.723646
8	28.47667	0.834777	24.43577	0.746466

Table3 shows that the performance of the existing and proposed method for 9 images with the PSNR and SSIM values for 20% Cartesian sampling rates.				
Method	**Existing method**		**Proposed MD-USLBPRNET**	
Image id	**PSNR**	**SSIM**	**PSNR**	**SSIM**
1	27.48748	0.723212	25.48388	0.634788
2	28.47757	0.697877	27.45778	0.621111
3	28.57744	0.724877	24.32746	0.654578
4	30.37643	0.818988	28.87788	0.776778
5	28.35626	0.824457	23.48584	0.803748
6	26.54777	0.673427	24.87883	0.656364
7	22.45747	0.759898	21.83743	0.725849
8	24.88878	0.736566	24.65747	0.708494

From the tables 1,2 and 3 the proposed MD-USLBPRNET method shows the values of PSNR and SSIM. These are better than the existing method for 20% radial sampling rates. And also this proposed architecture preserves the structural similarity.

Fig 3 shows that the result of the reconstruction images for that the LBP under-sampling image.

| Original Image | LBP under-sampled image | Reconstructed image |
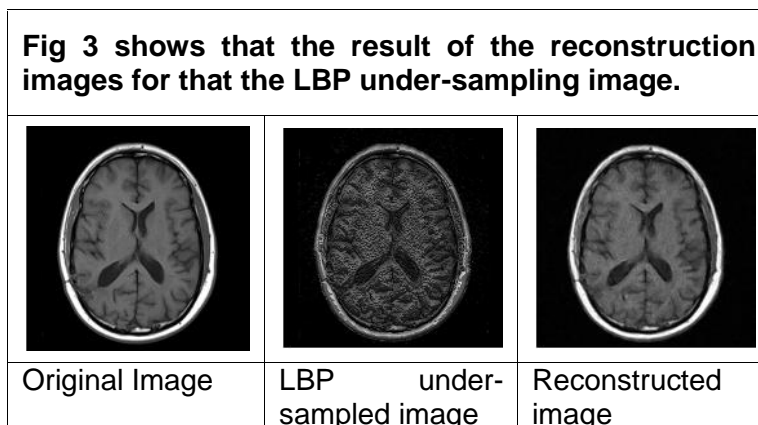
6. Conclusion

In this paper, our proposed MD-DLLBPRNET deals with the k-space and spatial data simultaneously. The proposed under-sampled data from k-space with local binary pattern and spatial domain are tested in this architecture. The experimental results demonstrate our proposed MD-DLLBPRNET can effectively preserve more detail at different sampling rates (10%, 20%, and 30%) with different sampling strategies (radial, Cartesian, and Gaussian random sampling). The extension of proposed MD-USLBPRNET architecture reconstructs and fusion the proposed under-sampled data with 20% radial sampling rates form spatial and k-space domain. This result shows the performance better than the existing method with the qualitative metric such as PSNR and SSIM.

References:
[1]   J. Bland, M. A. Belzunce, S. Ellis, C. J. McGinnity, A. Hammers, and A. J. Reader, "Spatially compact MRGuided kernel EM for PET image reconstruction," IEEE Trans. Radiat. Plasma Med. Sci., vol. 2, no. 5, pp. 470- 482, 2018.
[2]   D. L. Donoho, "Compressed sensing," *IEEE Transaction on Information Theory,* vol. 52, no. 4, 2006, pp. 1289–1306.
[3]   L. Gan, "Block compressed sensing of natural images," *IEEE International Conference on Digital Signal Processing ICDSP*, 2007, pp. 403–406.
[4]   S. S. Chen, D. L. Donoho, and M. A. Saunder , "Atomic decomposition by basis pursuit," *SIAM Journal of Scientific Computing.,* vol. 20, no. 1, 1999, pp. 33–61.
[5]   R. Baraniuk, M. Davenport, R. DeVore, and M.Wakin , "A simple proof of the restricted isometry property for random matrices," *Constructive Approximation*, vol. 28, no. 3, 2008, pp. 253–263.

[6]   J. Hamilton, D. Franson, and N. Seiberlich, "Recent advances in parallel imaging for MRI," Prog. Nucl. Magn. Reson. Spectrosc., vol. 101, pp. 71-95, 2017.
[7]   P. B. Roemer, W. A. Edelstein, C. E. Hayes, S. P. Souza, and O. M. Mueller, "The NMR phased array," Magn. Reson. Med., vol. 16, no. 2, pp. 192-225, 1990.
[8]   K. P. Pruessmann, M. Weiger, P. Börnert, and P. Boesiger, "Advances in sensitivity encoding with arbitrary k-space trajectories," Magn. Reson. Med., vol. 46, no. 4, pp. 638-651, 2001.

[9]   Y. J. Ma, W. Liu, X. Tang, and J. H. Gao, "Improved SENSE imaging using accurate coil sensitivity maps generated by a global magnitude-phase fitting method," Magn. Reson. Med., vol. 74, no. 1, pp. 217-224, 2015.

[10]   M. Bydder, D. J. Larkman, and J. V. Hajnal, "Generalized SMASH imaging," Magn. Reson. Med., vol. 47, no. 1, pp. 160-170, 2002.

[11]   M. A. Griswold et al., "Generalized autocalibrating partially parallel acquisitions (GRAPPA)," Magn. Reson. Med., vol. 47, no. 6, pp. 1202-1210, 2002.

[12]   W. E. Kyriakos et al., "Sensitivity profiles from an array of coils for encoding and reconstruction in parallel (SPACE RIP)," Magn. Reson. Med., vol. 44, no. 2, pp. 301-308, 2000.

[13]   M. Lustig and J. M. Pauly, "SPIRiT: iterative self - consistent parallel imaging reconstruction from arbitrary k-space," Magn. Reson. Med., vol. 64, no. 2, pp. 457- 471, 2010.

[14]   D. L. Donoho, "Compressed sensing," IEEE Trans. Inf. Theory, vol. 52, no. 4, pp. 1289-1306, 2006.

[15]   M. Lustig, D. L. Donoho, J. M. Santos, and J. M. Pauly, "Compressed sensing MRI," IEEE signal processing magazine, vol. 25, no. 2, p. 72, 2008.

[16]   M. Lustig, D. Donoho, and J. M. Pauly, "Sparse MRI: The application of compressed sensing for rapid MR imaging," Magn. Reson. Med., vol. 58, no. 6, pp. 1182- 1195, 2007.

[17]   J. Caballero, A. N. Price, D. Rueckert, and J. V. Hajnal, "Dictionary learning and time sparsity for dynamic MR data reconstruction," IEEE Trans. Med. Imaging, vol. 33, no. 4, pp. 979-994, 2014.

[18]   G. Yang et al., "DAGAN: deep de-aliasing generative adversarial networks for fast compressed sensing MRI reconstruction," IEEE Trans. Med. Imaging, vol. 37, no. 6, pp. 1310-1321, 2017.

[19]   T. M. Quan, T. Nguyen-Duc, and W.-K. Jeong, "Compressed sensing MRI reconstruction using a generative adversarial network with a cyclic loss," IEEE Trans. Med. Imaging, vol. 37, no. 6, pp. 1488-1497, 2018.

[20]   M. Mardani et al., "Deep generative adversarial neural networks for compressive sensing MRI," IEEE Trans. Med. Imaging, vol. 38, no. 1, pp. 167-179, 2018

[21]   Y. Han, L. Sunwoo, and J. C. Ye, "k-space deep learning for accelerated MRI," IEEE Trans. Med. Imaging, 2019.

[22]   Y. Yang, J. Sun, H. Li, and Z. Xu, "ADMM-CSNet: A Deep Learning Approach for Image Compressive Sensing," IEEE Trans. Pattern Anal. Mach. Intell., 2018.

[23]   J. Schlemper, J. Caballero, J. V. Hajnal, A. N. Price, and D. Rueckert, "A deep cascade of convolutional neural networks for dynamic MR image reconstruction," IEEE Trans. Med. Imaging, vol. 37, no. 2, pp. 491-503, 2017.

[24]   J. Schlemper et al., "Stochastic deep compressive sensing for the reconstruction of diffusion tensor cardiac MRI," in International conference on medical image computing and computer-assisted intervention, 2018: Springer, pp. 295-303.

[25]   B. Zhu, J. Z. Liu, S. F. Cauley, B. R. Rosen, and M. S. Rosen, "Image reconstruction by domain-transform manifold learning," Nature, vol. 555, no. 7697, p. 487, 2018.

[26]   S. Wang et al., "DIMENSION: Dynamic MR imaging with both k-space and spatial prior knowledge obtained via multi-supervised network training," NMR Biomed., 2018.

[27]   T. Eo, Y. Jun, T. Kim, J. Jang, H. J. Lee, and D. Hwang, "KIKI - net: cross - domain convolutional neural networks for reconstructing under-sampled magnetic resonance images," Magn. Reson. Med., vol. 80, no. 5, pp. 2188-2201, 2018.

[28]   D.M. Christilin, A. Brighty, M.S. Mary, Compressed Sensing Reconstruction based on Adaptive Scale Parameter using Texture Feature. Int. J. Innov. Technol. Explor. Eng. 8(12) (2019), 5455–5461.

[29]   D. Lee, J. Yoo, S. Tak, and J. C. Ye, "Deep residual learning for accelerated MRI using magnitude and phase networks," IEEE Trans. Biomed. Eng., vol. 65, no. 9, pp. 1985-1995, 2018.

[30]   K. He, X. Zhang, S. Ren, and J. Sun, "Deep residual learning for image recognition," in Proceedings of the IEEE conference on computer vision and pattern recognition (CVPR), 2016, pp. 770-778.